Miyake T, Sawada A, Yamamoto T, Miyake K, Sugiyama K, Kitazawa Y.	The incidence of disc hemorrhage in open-angle glaucoma before and after trabeculectomy.	J Glaucoma	15 (2)	164-171	2006
Hara A, Niwa M, Kumada M, Aoki H, Kunisada T, Oyama T, Yamamoto T, Kozawa O, Mori H.	Intraocular injection of folate antagonist methotrexate induces neuronal differentiation of embryonic stem cells transplanted in the adult mouse retina.	Brain Res	1085	33-42	2006
Karim MZ, Sawada A, Kawakami H, Yamamoto T, Taniguchi T	A new calcium channel antagonist, lomerizine, alleviates secondary retinal ganglion cell death after optic nerve injury in the rat.	Curr Eye Res	31	273-283	2006
Suemori S, Shimazawa M, Kawase K, Satoh M, Nagase H, Yamamoto T, Hara H.	Metallothionein, an endogenous antioxidant, protects against retinal neuron damage in mice.	Invest Ophthalmol Vis Sci	47(9)	3975-3982	2006
Hasegawa K, Ishida K, Sawada A, Kawase K, Yamamoto T.	Diurnal variation of intraocular pressure in suspected normal-tension glaucoma.	Jpn J Ophthalmol	50(5)	449-454	2006
Hara A, Niwa M, Aoki H, Kumada M, Aoki H, Kunisada T, Oyama T, Yamamoto T, Kozawa O, Mori H:	A new model of retinal photoreceptor cell degeneration induced by a chemical hypoxia-mimicking agent, cobalt chloride.	Brain Res	1109(1)	192-200	2006
Ohkubo S, Takada H, Higashide T, Sasaki T, Sugiyama K.	A pilot study to detect glaucoma with confocal scanning laser ophthalmoscopy compared to nonmydriatic stereoscopic photography in a community health screening.	J Glaucoma		in press	
Kawaguchi I, Higashide T, Ohkubo S, Takeda H, Sugiyama K.	In vivo imaging and quantitative evaluation of the rat retinal nerve fiber layer using scanning laser ophthalmoscopy.	Invest Ophthalmol Vis Sci	47(7)	2911-2916	2006
Higashide T, Kawaguchi I, Ohkubo S, Takeda H, Sugiyama K.	In vivo imaging and counting of rat retinal ganglion cells using a scanning laser ophthalmoscope.	Invest Ophthalmol Vis Sci	47(7)	2943-2950	2006
Goseki T, Ishikawa H, Nishimoto H, Mashimo K, Uga S, Yoshitomi T, Shimizu K.	Pharmacological vascular reactivity in isolated diabetic rabbit ciliary artery.	Exp Eye Res	83	1317-1324	2006
Dong Y, Ishikawa H, Wu Y, Shimizu K, Goseki T, Yoshitomi T.	Effect and mechanism of Betaxolol and Timolol on Vascular Relaxation in Isolated Rabbit Ciliary Artery.	Jpn J Ophthalmol	50	504–508	2006
Dong Y, Ishikawa H , Wu Y, Yoshitomi T.	Vasodilatory mechanism of levobunolol on vascular smooth muscle cells.	Exp Eye Res		in press	
Saito H, Tomidokoro A, Sugimoto E, Aihara M, Tomita G, Fujie K, Wakakura M, Araie M.	Optic disc topography and peripapillary retinal nerve fiber layer thickness in nonarteritic ischemic optic neuropathy and open-angle glaucoma.	Ophthalmology	113	1340-1344	2006
Kunimatsu S, Tomidokoro A, Saito H, Aihara M, Tomita G, Araie M.	Performance of GDx VCC in eyes with peripapillary atrophy: comparison of three circle sizes.	Eye	Aug 4	[Epub ahead of print]	2006
Kawano J, Tomidokoro A, Mayama C, Kunimatsu S, Tomita G, Araie M.	Correlation between hemifield visual field damage and corresponding parapapillary atrophy in normal-tension glaucoma.	Am J Ophthalmol	142	40-45	2006

あたらしい眼科 24(1)：51～57，2007

視神経乳頭観察法の進歩（緑内障を中心に）

Development of Optic Disc Evaluation in Glaucoma

大久保真司* 杉山和久*

はじめに

視神経乳頭観察は眼科医の診察の基本であり，基本的な観察方法に大きな変化はない．視神経乳頭を観察するポイントとして，視神経に異型性がないか色調がどうであるかなどの平面的な情報だけでなく，視神経乳頭が隆起しているかあるいは陥凹がないかといった立体的な評価をする必要がある．

特に緑内障の診断と経過観察には，視神経乳頭の緑内障性変化を的確に評価することが最も重要である．多治見スタディの結果[1]，日本人には正常眼圧緑内障が多いことが明らかになり，緑内障スクリーニングにおける視神経乳頭観察の重要性も増してきている．しかし，視神経乳頭観察は主観的で経験に左右される．定量性がないために視神経乳頭による病期分類や経過の比較が困難である．そのため，視神経乳頭評価の数字化や，ステージングを行うことが試みられてきた．今回，視神経乳頭観察と，その評価法の進歩に関して緑内障を中心に述べたい．

近年，視神経乳頭を客観的に定量的に評価するためにさまざまな検査機器が開発されている．これらの代表的な機器として，Heidelberg Retina Tomograph II（HRT II；Heidelberg Instruments, Dossenheim, Germany）およびOptical Coherence Tomography 3000（OCT 3；Carl Zeiss Meditec, Dublin, CA）の視神経乳頭解析について簡単に解説したい．

I 視神経乳頭観察法

視神経乳頭の観察方法としては，倒像鏡，直像鏡および細隙灯顕微鏡を用いた方法がある．しかし，通常の倒像鏡による眼底検査では像が小さく視神経乳頭の詳細な観察には不向きである．いずれの場合も散瞳して観察を行うことが望ましいが，さまざまな事情で散瞳できない場合も多い．非散瞳下では直像鏡が有用である．直像鏡では視神経乳頭の拡大率が大きく詳細な観察が可能である．直像鏡は単眼での平面的な観察ではあるが，視線の方向を変えながら，血管の屈曲点を注意深く観察することによりかなり正確に乳頭辺縁部（リム）を同定できる．90DやSuper fieldなどの非接触型前置レンズやGoldmann三面鏡，隅角鏡でも非散瞳下のリムをある程度立体的に把握できる．さらに，ステレオバリエータのついているタイプでは，これを用いることにより像は平坦化するが小瞳孔でも立体視が得やすい．立体視が得られない場合でも，スリット光を動かしながら観察することによりある程度陥凹を把握することが可能である．散瞳下では，Goldmann三面鏡，隅角鏡，非接触型前置レンズなどを症例および状況に応じて使用し，立体的に視神経乳頭の観察を行う．

1．細隙灯顕微鏡を用いた眼底検査における使用レンズの特性

細隙灯顕微鏡を用いた眼底検査を行う際に使用するレ

* Shinji Ohkubo & Kazuhisa Sugiyama：金沢大学大学院医学系研究科視覚科学
〔別刷請求先〕大久保真司：〒920-8641 金沢市宝町13-1 金沢大学大学院医学系研究科視覚科学

0910-1810/07/¥100/頁/JCLS

ンズの特性を理解しておく必要がある．眼底観察像の大きさ（横倍率）は眼の全屈折力（60D）と前置レンズの屈折力の比でほぼ決定される．たとえば，90Dレンズを用いた倒像鏡検査では眼底像は約2/3倍になる．眼底の凹凸など観察方向の倍率（縦倍率）は横倍率の2乗に比例するので，眼球に接触させずに手軽に使用できる90DやSuper fieldでは，視神経乳頭の陥凹は実際の約1/2となり初期の微妙な陥凹を観察評価するには適さない．それに対してGoldmann三面鏡や隅角鏡は縦倍率が1倍で陥凹の詳細な観察に適する．ここで忘れてならないのは，細隙灯顕微鏡の倍率を上げてもレンズの解像度を代償することはできないことである．すなわち低倍率の前置レンズを使用した場合，いくら細隙灯顕微鏡の倍率を上げても高い解像度の像を得ることはできない．

2．緑内障診療における視神経乳頭観察のポイント

視神経乳頭陥凹を評価する際，平面的に乳頭の色調のみから陥凹の大きさを判断すると早期の緑内障ではその評価を誤る可能性があり，必ず立体的に評価する．乳頭陥凹は一般に視神経乳頭が大きいほど大きいので，大きい乳頭では過大評価されやすい．したがって，乳頭陥凹の大きさよりもむしろリムの厚みに注目し，視神経乳頭を観察する．

実際の緑内障診療における視神経乳頭の観察においては乳頭陥凹の大きさ，リムの厚みだけではなく乳頭陥凹の左右差（水平cup/disc比の左右差が0.2より大きいことは正常人の3%以下であるとされている），notching（乳頭辺縁の局所的な菲薄化），乳頭上網膜血管の鼻側偏位，視神経乳頭の線状出血および乳頭周囲の網脈絡膜萎縮（peripapillary atrophy：PPA）などに注意する．また視神経乳頭のみならず網膜神経線維層欠損（nerve fiber layer defect：NFLD）がないか注意して観察する．小さい視神経乳頭など緑内障性変化を評価しにくい場合には，NFLDなど網膜神経線維の変化の観察が有用である（図1）．

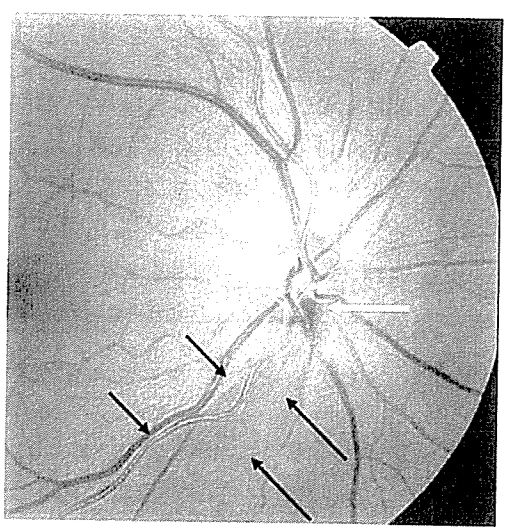

図1　右緑内障眼の眼底写真
視神経乳頭は小さく，乳頭陥凹の判定は困難である．網膜神経線維層欠損（黒矢印で囲まれた部位）とその境界に視神経乳頭出血（白矢印）がみられる．

II　眼底写真

通常の平面的な眼底写真でも注意深く血管の屈曲点を追うことで乳頭陥凹を評価できる．しかし，血管のない部位の評価が困難であること，乳頭鼻側の陥凹拡大を見落としやすいことなどの欠点がある．ステレオ眼底写真は，視神経乳頭を立体的に観察することができ診断および経過観察に役立つ．撮影角度の変わらない同時撮影のステレオ眼底写真が理想的であるが，通常のカメラでも左右に少し移動して片眼を2枚撮影することによってステレオ眼底写真を撮影することができる（図2，3a）．し

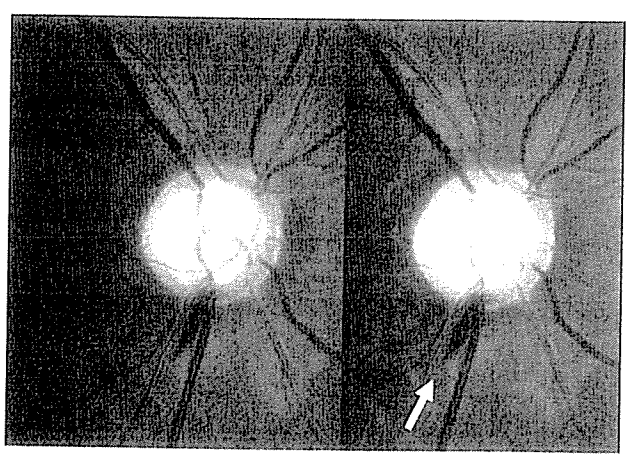

図2　右緑内障眼のステレオ眼底写真（平行移動法）
ステレオ眼底写真を用いることで視神経乳頭陥凹を立体的に観察することができる．6時半に視神経乳頭出血（白矢印）を認める．

かし，同時撮影でない場合は常に撮影角度が一定とはいえないので，正確に視神経乳頭の経時的な立体的変化を評価することは困難である．

また，最近ではコンピュータのソフトと特殊なメガネを使用してステレオ眼底写真を観察するビューワーシステムが開発されており，大量に眼底写真の読影が必要な際に重宝する．

III　視神経乳頭変化の定量化

緑内障診療において①診断（健常か緑内障かの鑑別），②おおまかな病期分類，③経過観察（進行したかどうかを判断する）ために，視神経乳頭変化を定量化する必要がある．

1. Cup-to-disc ratio（C/D 比）

1960 年代に Armaly[2] が報告した C/D 比は，視神経乳頭のダメージを定量的に評価した最初の指標であり，非常に簡単で使いやすいために普及し，現在も広く用いられている．一般的に C/D 比が大きいほど，緑内障が疑われるが，実際には C/D 比が大きくとも緑内障でない人もいれば，C/D 比が大きくなくても緑内障の人もいる．正常人の平均 C/D 比は緑内障患者の平均 C/D 比より小さいが，C/D 比は両群ともばらつきが大きくて，かなりの人がオーバーラップする[3]．よって垂直および水平 C/D 比のみでは，特に早期の緑内障診断は困難である．

C/D 比での緑内障診断を困難にしている原因はおもに①C/D 比は中心を測定するので，乳頭陥凹の同心円性の拡大は正確に評価できるが，緑内障の場合は偏心して乳頭陥凹の変化を起こすことも多い，②notching などの局所的な変化を反映しない，③健常人において視神経乳頭線維の数が同じとすれば，リムの面積は同じになるが，視神経乳頭が小さければ C/D 比は小さくなり，視神経乳頭が大きくなれば C/D 比は大きくなる，以上の 3 点が考えられている．

用語解説

C/D 比（cup-to-disc ratio）：通常視神経乳頭の中央は凹んでおり，乳頭陥凹とよばれる．乳頭陥凹の大きさをある経線上の端から端で計測（陥凹径）して，その同一線上での乳頭径に対する比である．Armaly の定義では，C/D 比といえば横径を計測する水平 C/D 比であるが，初期の緑内障変化は陥凹の垂直方向の変化から起こることが多く，緑内障性変化を評価する際には縦径を計測する垂直 C/D 比が重要である．

2. The Disk Damage Likelihood Scale（DDLS）

近年 C/D 比での問題点を解決すべく，The Disk Damage Likelihood Scale（DDLS）というシステムが報告されている[4]．このシステムは少しずつ改変されており，9 段階に分類されたバージョンに関する論文が最も多いが，10 段階に分類される最新バージョン[5] が最も単純でわかりやすい．このシステムは，いずれの部位であっても最も薄い幅のリム/乳頭比に基づいて決められ，さらにリムが消失している場合はリムの消失している角度で評価される．具体的には，視神経乳頭径が 1.5 mm から 2.00 mm の平均的な大きさの場合，DDLS のステージ 1 は最も狭いリム/乳頭比が 0.4 以上，同様にステージ 2 は最も狭いリム/乳頭比が 0.3 から 0.39，ステージ 3 では最も狭いリム/乳頭比が 0.2 から 0.29，ステージ 4 では最も狭いリム/乳頭比が 0.1 から 0.19，ステージ 5 では最も狭いリム/乳頭比が 0.1 以下（0 ではない）である．リム/乳頭比が 0 すなわち，いずれかの場所でリムが消失している場合はステージ 6 から 10 に分類される．リムが消失している角度が 45°未満の場合はステージ 6，46°から 90°の場合はステージ 7，91°から 180°の場合はステージ 8，181°から 270°の場合はステージ 9，270°以上の場合はステージ 10 に分類される．この際耳側のリムの評価には注意を要する．すなわち，傾斜しているリムを，リムの消失と誤らないようにしなければならない．さらに視神経乳頭の大きさを考慮して，小さい視神経乳頭（乳頭径<1.5 mm）の場合ステージを 1 段階上げ，大きい視神経乳頭（乳頭径>2.0 mm）の場合ステージを 1 段階下げる．ちなみに視神経乳頭径は，60 D から 90 D のレンズを用いて測定し，レンズごとに決まった値の補正値を使用して求める．

DDLS の欠点としては，リムが狭細化している場所が考慮されていない点および連続していないリムの狭細化

があった場合，狭い部位に関しては考慮されない点があげられる．また先天奇形を伴った視神経乳頭など分類が困難な視神経乳頭を，評価することは困難である．このシステムは，C/D比に比べてやや複雑であるが，基本的な考え方としては，緑内障を評価する際には，乳頭陥凹の大きさよりもむしろリムの厚みに注目し，視神経乳頭を観察するという原則や，緑内障性変化は小さい乳頭では過少評価され，大きい乳頭では過大評価されやすい点を考慮している点はわれわれが通常診療において常に気をつけている点と一致している．しかし，C/D比にしろDDLSにしろいずれの評価法においても，評価は主観的で観察者に依存する．その点を克服するために，画像解析装置が用いられてきている．

IV　最近の画像解析装置（HRTおよびOCT）

視神経乳頭を定量的に評価して客観的に緑内障を診断し，経過観察を行うための手段として，近年Heidelberg Retina Tomograph（HRT；Heidelberg Engineering, Dossenheim, Germany）と光干渉断層計（Optical Coherence Tomography：OCT；Carl Zeiss Meditec, Dublin, CA）などが用いられてきている（症例呈示：図3a～d）．

1. Heidelberg Retina Tomograph II（HRT II）

HRTは波長670 nmのダイオードレーザーを使用した共焦点レーザー走査型顕微鏡で，優れた測定再現性および乳頭パラメータの信頼性をもつ画像解析装置である．近年HRTの普及型として解析部位を視神経乳頭に絞り，撮影画角のサイズを15°×15°に固定したHRT IIが導入された．

HRT IIでは検査にあたって散瞳する必要はなく，内部固視灯を被検者が固視するとちょうど画面の中央に視神経乳頭が位置するように設定されている．検査眼のフォーカスを合わせて一度操作ボタンを押すだけでHRT IIは自動的にスキャン幅を決定し，その後3回連続して画像を取り込み，面倒な設定なしに短時間で平均画像を得ることができる．取り込んだ画像は16から64枚の連続的で等距離（1/16 mm）の二次元のシリーズ画像で構成され，各二次元画像は384×384ピクセルの解像度をもつ．コンピュータがその画像を立体的に再構築し，三次元解析が可能となる．検者が測定画面上で視神経乳頭縁（コントアライン）を決定すると，自動的にコントアラインに沿った網膜表面の高さが得られる（図

図3　左緑内障眼のステレオ眼底写真（a），HRT II解析結果（b），OCT 3のOptic Nerve Head解析画面（c）およびHumphrey視野（d）

a：乳頭陥凹は拡大しており，5時から6時のリムは完全に消失している（白両矢印）．明瞭ではないが，2時と5時に網膜神経線維層欠損（NFLD）（黒矢印で囲まれた部位）がみられる．

b：ベースライン検査では，トポグラフィ画像（**上段左**），反射画像（**上段右**），Y軸高さプロファイル（**上段中央**），X軸高さプロファイル（**中段左**），コントアラインの高さ変化（**中段右**），立体計測パラメータ（**下段左**）およびMoorfields回帰解析結果（**下段右**）が表示される．トポグラフィ画像は，各測定点における眼底表面の高さを表している．明部は凹部，暗部は凸部を表している．さらに乳頭には赤/青/緑のオーバーレイを表示．赤の領域は視神経乳頭の陥凹領域で，乳頭の残りのリム領域は，傾斜部（青）と平らな部分（緑）に分けられる．反射画像は，各測定点の反射率を表示．明るい部分はより多くの反射光がカメラに戻ってきた場所を示す．さらに視神経乳頭を6分割して各セクターのMoorfields回帰解析判定結果を重ねて表示．Moorfields回帰解析判定が“within normal limits”，“borderline”，“outside normal limits”であれば，それぞれ緑色のチェックマーク，黄色の感嘆符，赤い×印が表示される．コントアラインの高さは耳側，上側，鼻側，下側の順に展開した曲線として表示（**中段右**）．この症例ではMoorfields回帰解析は“Outside normal limits”（**下段右**）．HRT IIで測定した視神経乳頭サイズ（Disk Area）2.234 mm^2，垂直C/D比（Linear Cup/Disk Ratio）は0.792（**下段左**）．

c：画面左にスキャン画像（この図では垂直方向のスキャン），その下に眼底画像が表示される．スキャン画像中のライトブルーの円内のライトブルーの2本の直線の交点（白矢印）が網膜色素上皮の終結する参照点．この2点の参照点間を結んだ直線が乳頭径と定義される．この直線に対して150 μm前方に平行する赤点線（赤矢印）より高い位置がリム（赤の凝縮された部位），低い位置が陥凹とされる．画面右側の表示は視神経乳頭解析画像で，6本の放射状スキャン画像から構築される視神経乳頭の合成画像．赤線で囲まれた円の内部がDisk Area，緑線で囲まれた円の内部がCup Area．OCT 3で測定した視神経乳頭サイズ（Disk Area）2.394 mm^2，垂直C/D比（Cup/Disk Vert. Ratio）は0.885（**下段右**）．

d：Humphrey視野では，下方のリム消失に対応した上方の視野変化および2時のNFLDに対応すると思われる下方の視野変化（グレースケールでは，はっきりしないが，パターン偏差では明瞭となっている）がみられる．HfaFiles Ver5（Beeline Office Co. Japan）によるプリントアウト．

3b 中段右）．耳側 350°～356°のセクターにみられる乳頭黄斑束部のコントアラインの平均の高さより 50 μm 低い位置は，神経線維層の底の部分とほぼ同じ位置になり，その線がリファレンスプレーンの位置となる．リファレンスプレーンより上がリム，リファレンスプレーンより下が陥凹と定義される．

HRT II では視神経乳頭に関する多くのパラメータが表示されるとともに，視神経乳頭の緑内障性変化の有無を判定する自動診断プログラムが付属されている．視神経乳頭を 6 セクターに分け，Wollstein ら[6] が報告した Moorfields の回帰解析に基づき全体と各セクターでのリム面積と乳頭領域の面積比を評価することにより，“within normal limits”，“borderline”，“outside normal limits” の 3 段階で判定する（図 3b の下段右）．

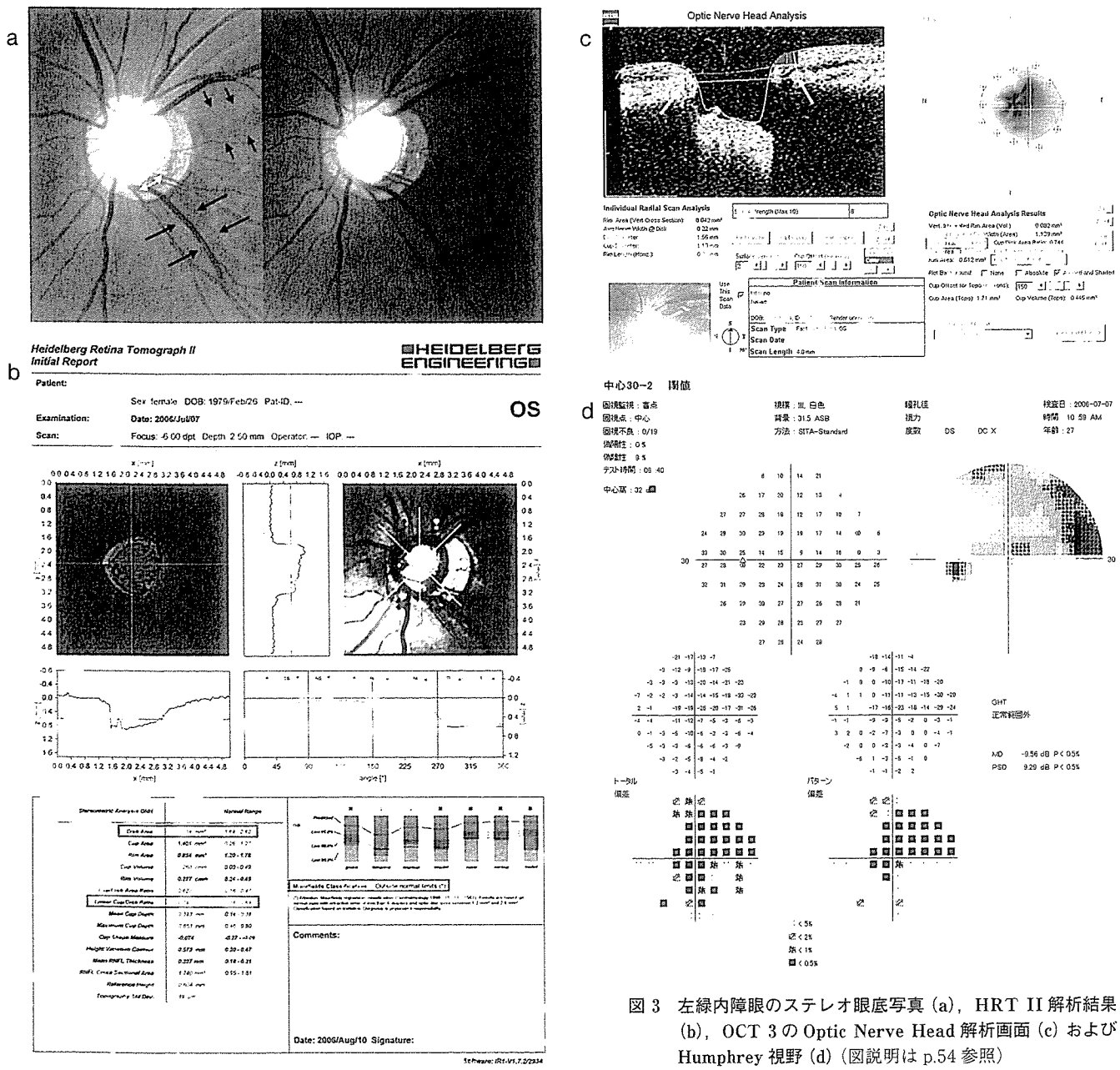

図 3　左緑内障眼のステレオ眼底写真 (a)，HRT II 解析結果 (b)，OCT 3 の Optic Nerve Head 解析画面 (c) および Humphrey 視野 (d)（図説明は p.54 参照）

2. Optical Coherence Tomography 3000 (OCT 3)

近年OCTも，緑内障診断に用いられている．OCTは従来の超音波を用いた画像診断と類似の原理に基づく測定機器であり，超音波の代わりにダイオード光源による波長820 nmの近赤外線低干渉光を用いるため，非侵襲的に高い解像度の画像が得られ，OCT 3では縦断面，横断面ともに10 μmの解像度が得られる．OCT 3では，検査可能な被検者の最小瞳孔径が3.2 mmとなったので，無散瞳でも検査可能になった．

OCT 3には，緑内障診断補助プログラムとして，RNFL Thickness Average（網膜神経線維層厚解析），RNFL Thickness Map（網膜神経線維層厚マップ），Optic Nerve Head Analysis（視神経乳頭解析）がある．

そのなかで乳頭解析プログラムとしてはOptic Nerve Head Analysis（視神経乳頭解析）があり，視神経乳頭を4 mmの放射状ラインで6本スキャンして得られる結果から，水平・垂直C/D比，リム面積・体積，カップ径，陥凹の深さなどが自動的に計測解析される（図3c）．この解析では反射輝度の特定の閾値を検索することによって神経線維層前面と網膜色素上皮を検出する．解剖学的に網膜色素上皮が終結する視神経乳頭の両端が解剖学的マーカー（参照点）として決定され，この2点が視神経乳頭の全解析の基本となる．視神経乳頭両端の2点の参照点間を直線で結ぶことにより乳頭径が求められる．この直線に対して150 μm前方に平行する赤点線より高い位置がリム，低い位置が陥凹とされる．これらは客観的に自動的に計算されるが，手動で参照点を調整することができる．

OCT 3では，解像度は低いが6本のラインスキャンを1.92秒で一度に捉えることができるfast scansというシステムが導入された．通常の高解像度のスキャンでは1本のラインのスキャンに1.28秒かかり，これを少なくとも6本測定しなければならない．Kamppeter ら[7]は，正常人を通常のモード（Optical Disc），fast scansモード（Fast Optical Disc）の2つのモードで測定し，それぞれにおいて自動で参照点を決めて計算した場合と，参照点を手動で修正した場合で再現性について検討し，通常のモードで修正しなかった場合はアーチファクトのため良いデータが得られず，fast scansモードで参照点を手動で修正した場合が最も再現性が高かったと報告している．その理由として，1本ずつ捉えるパターンでは全スキャンが終了するまで時間がかかり，その間患者の固視移動，スキャン部位の移動などで解析結果にばらつきが生じるためと思われる．

3. HRT IIとOCT 3の測定値の比較（図3）

近年それぞれの測定値の関係について検討されてきている．HRT IIとOCT 3で測定した視神経乳頭面積は高い相関があるが，HRT IIで測定した平均の視神経乳頭面積は，OCTで測定した乳頭面積よりいずれの視神経乳頭サイズでも常に小さい傾向にあるようだ[8,9]．Arthur ら[10]は，水平C/D比と垂直C/D比について，同時撮影ステレオ眼底写真，HRT II，OCT 3で比較し，OCT 3が水平C/D比と垂直C/D比ともに最も大きく，水平C/D比が最も小さかったのは同時撮影ステレオ眼底写真で，垂直C/D比が最も小さかったのはHRT IIであったと報告している．水平C/D比と垂直C/D比ともにOCTは陥凹の最長径に対する視神経乳頭最長径の比率を計算しているのに対して，HRT IIでは視神経乳頭の中心でC/D比を測定している．この点が，OCTのC/D比が，HRT IIのC/D比より大きい理由の一つと考察されている．各機器で測定された各パラメータはそれぞれよく相関しているが，それぞれの機器のデータの互換性は今のところないので，同一機種間での経過観察には使用できるが，各パラメータを比較する際には注意を要する．

おわりに

いかに画像解析装置が進歩しようとも，視神経乳頭を立体的に観察することは緑内障診療の基本であり，視神経乳頭を常に立体的に観察する習慣をつける必要がある．C/D比なり，DDLSなり自分なりの視神経乳頭変化の定量化システムをもつことは，緑内障の診断，病期分類および経過観察の際に重宝する．最新の画像解析装置は再現性も信頼性も高く，客観的に定量化することができ，診断および経過観察の心強い補助診断機器と思われる．

文　献

1) Iwase A, Suzuki Y, Araie M et al : The prevalence of primary open-angle glaucoma in Japanese. *Ophthalmology* **111** : 1641-1648, 2004
2) Armaly MF : The optic cup in the normal eye. I. Cup width, depth, vessel displacement, ocular tension and outflow facility. *Am J Ophthalmol* **68** : 401-407, 1969
3) Caprioli J, Miller JM : Videographic measurements of optic nerve topography in glaucoma. *Invest Ophthalmol Vis Sci* **29** : 1294-1298, 1988
4) Bayer A, Harasymowycz P, Henderer JD et al : Validity of a new disk grading scale for estimating glaucomatous damage : correlation with visual field damage. *Am J Ophthalmol* **133** : 758-763, 2002
5) Spaeth GL, Lopes JF, Junk AK et al : System for staging the amount of optic nerve damage in glaucoma : a criteria review and new material. *Surv Ophthalmol* **51** : 293-315, 2006
6) Wollstein G, Garway-Heath DF, Hitchings RA : Identification of early glaucoma cases with the scanning laser ophthalmoscope. *Ophthalmology* **105** : 1557-1563, 1998
7) Kamppeter BA, Schubert KV, Budde WM et al : Optical coherence tomography of the optic nerve head : interindividual reproducibility. *J Glaucoma* **15** : 248-254, 2006
8) Hoffmann EM, Bowd C, Medeiros FA et al : Agreement among 3 optical imaging methods for the assessment of optic disc topography. *Ophthalmology* **112** : 2149-2156, 2005
9) Schuman JS, Wollstein G, Farra T et al : Comparison of optic nerve head measurements obtained by optical coherence tomography and confocal scanning laser ophthalmoscopy. *Am J Ophthalmol* **135** : 504-512, 2003
10) Arthur SN, Aldridge AJ, De Leon-Ortega J et al : Agreement in assessing cup-to-disc ratio measurement among stereoscopic optic nerve head photographs, HRT II, and Stratus OCT. *J Glaucoma* **15** : 183-189, 2006

Journal of Neurochemistry, 2006, **96**, 43–52 doi:10.1111/j.1471-4159.2005.03502.x

NMDA-induced retinal injury is mediated by an endoplasmic reticulum stress-related protein, CHOP/GADD153

Maiko Awai,*[,1] Takahisa Koga,*[,†,1] Yasuya Inomata,* Seiichi Oyadomari,† Tomomi Gotoh,† Masataka Mori† and Hidenobu Tanihara*

*Departments of *Ophthalmology and Visual Science and †Molecular Genetics, Kumamoto University Graduate School of Medical Sciences, Kumamoto, Japan*

Abstract

We investigated the role of an endoplasmic reticulum stress-associated protein, CHOP/GADD153, after NMDA-induced mouse retinal damage. After injection of NMDA into the vitreous, TUNEL-positive cells were detected in the retinal ganglion cell layer (GCL) and inner nuclear layer (INL) at 6 h after NMDA injection, and these gradually increased in number up to 24 h. Analysis by real-time RT-PCR revealed that CHOP mRNA was induced by about 3-fold, at 2 h after NMDA injection. Immunoreactivity for the CHOP protein was intense in cells of the GCL following NMDA treatment. Immunoblot analysis showed that NMDA injection increased the expression of CHOP protein in the retina. Compared with wild-type mice, $CHOP^{-/-}$ mice were more resistant to NMDA-induced retinal cell death as determined by TUNEL assay. At 7 days after NMDA treatment, the thickness of the inner plexiform layer and INL were larger in $CHOP^{-/-}$ mice than in wild-type mice. The number of residual cells in the GCL following NMDA treatment was significantly higher in $CHOP^{-/-}$ mice than in wild-type mice. In conclusion, CHOP is induced in mouse retina by NMDA treatment, and $CHOP^{-/-}$ mice are more resistant to NMDA-induced retinal damage, suggesting that CHOP plays an important role in NMDA-induced retinal cell death.

Keywords: C/EBP homologous protein, endoplasmic reticulum, NMDA, retinal ganglion cells.

J. Neurochem. (2006) **96**, 43–52.

Apoptotic cell death is associated with various retinal disorders, including human and experimental retinitis pigmentosa (Reme *et al.* 1998; Farrar *et al.* 2002), retinal ischaemia of animal model (Kuroiwa *et al.* 1998; Rosenbaum *et al.* 1998), and experimental glaucoma (Quigley *et al.* 1995) and human glaucoma (Kerrigan *et al.* 1997; Wax *et al.* 1998). Glutamate, an excitatory amino acid, causes retinal neuronal cell death. The *N*-methyl-D-aspartate (NMDA) receptor, which is one of the glutamate receptors, has been implicated in retinal neuronal cell death (Lam *et al.* 1999a). Administration of NMDA into animal vitreous cavities induced cell death in the ganglion cell layer (GCL) and inner nuclear layer (INL) of the retina (Joo *et al.* 1999). This retinal injury model has been widely used to investigate the mechanism of retinal neuronal cell death and to investigate neuroprotective factors and drugs (Inomata *et al.* 2003a,b).

The endoplasmic reticulum (ER) is an intracellular Ca^{2+} storage compartment in most cells. In the ER, newly synthesized 'secretary' proteins undergo glycosylation, disulfide bond formation, folding and oligomerization. These activities strictly depend on a high Ca^{2+} concentration in the ER (Alberts *et al.* 2002). Exposure of neurons to glutamate activates glutamate receptors and raises cytosolic Ca^{2+} levels.

Received April 21, 2005; revised manuscript received July 19, 2005; accepted August 22, 2005.

Address correspondence and reprint requests to Hidenobu Tanihara MD, Department of Ophthalmology, Kumamoto University School of Medicine, 1-1-1 Honjo, Kumamoto, 860–8556, Japan.
E-mail: tanihara@pearl.ocn.ne.jp

[1]These authors contributed equally to this work.

Abbreviations used: ARVO, Association for Research in Vision and Ophthalmology; ASK, apoptosis signal-regulating kinase; CHOP, C/EBP homologous protein; ECL, enhanced chemiluminescence; ER, endoplasmic reticulum; GADD153, growth arrest and DNA damage-inducible gene 153; GAPDH, glyceraldehyde-3-phosphate dehydrogenase; GCL, ganglion cell layer; HRP, horseradish peroxidase; INL, inner nuclear layer; NIH, National Institutes of Health; PAGE, polyacrylamide gel electrophoresis; PBS, phosphate-buffered saline; PI, propidium iodide; RGCs, retinal ganglion cells; SDS, sodium dodecyl sulfate; TBS, Tris-buffered saline; TSA, tyramide signal amplification; TUNEL, terminal deoxyribonucleotidyl transferase (TdT)-mediated fluroscein-16-dUTP nick-end labelling.

Ca^{2+} first enters the cytosol from the extracellular space through glutamate receptors, and then a large amount of Ca^{2+} is released from the ER to the cytosol (Paschen and Frandsen 2001; Hajnoczky *et al.* 2003). Disturbance of Ca^{2+} homeostasis in the ER leads to its dysfunction. Other conditions such as hypoxia, hypoglycaemia, and mutation of 'secretory' protein genes induce ER dysfunction and ER stress (Kaufman *et al.* 2002; Oyadomari *et al.* 2002a,b; Oyadomari and Mori 2004). When cells experience severe ER stress, the C/EBP homologous protein (CHOP), also known as growth arrest and DNA damage-inducible gene 153 (GADD 153), is induced in certain cell types (Ron and Habener 1992; Barone *et al.* 1994; Oyadomari *et al.* 2002a,b). CHOP is expressed at low levels under physiological conditions and is highly induced in response to ER stress (Ron *et al.* 1992). Induction of CHOP plays a key role in the pathway of ER stress-mediated apoptosis (Kawahara *et al.* 2001; Oyadomari *et al.* 2001; Gotoh *et al.* 2002; Oyadomari *et al.* 2002a,b; Gotoh *et al.* 2004; Oyadomari *et al.* 2004; Tajiri *et al.* 2004; Tsutsumi *et al.* 2004).

In this study, we report that CHOP is induced in cells of the GCL following NMDA treatment and that CHOP-deficient mice are more resistant to NMDA-induced retinal neuronal cell death.

Materials and methods

NMDA-induced retinal injury

All experiments conformed to the ARVO Statement for the Use of Animals in Ophthalmic and Vision Research. $CHOP^{-/-}$ mice (C57 BL/6 background) were provided by Dr Shizuo Akira (Osaka University, Japan). C57 BL/6 and $CHOP^{-/-}$ male mice, 8–12 weeks old, were used in this study. Mice were anaesthetized by intramuscular injection of 0.025 mg of ketamine hydrochloride (Sankyo, Tokyo, Japan) and 0.1 mg of xylazine (Bayer, Leverkusen, Germany). After the pupil was dilated with phenylephrine hydrochloride and tropicamide, injection into the vitreous cavity was performed under a microscope using a 33-gauge needle connected to a microsyringe and inserted toward to the posterior pole carefully, and not inserted too deep to avoid lens damage, approximately 1 mm behind the corneal limbus. NMDA and NMDA antagonst, MK-801 were obtained from Sigma (St Louis, MO, USA). A single dose of 2 mL of sterilized phosphate-buffered saline (PBS) containing NMDA was injected into the vitreous cavity. Some mice were systemically treated with 0.01 mg of MK-801 through a single injection into the peritoneal cavity 1 h before intravitreous NMDA injection. Control mice received either no injection or an injection of 2 mL of PBS into the vitreous cavity.

Real-time reverse transcription-polymerase chain reaction (RT-PCR) of CHOP mRNA

NMDA (5 nmol/2 mL) was injected into the vitreous cavity in C57 BL/6 mice. At 2, 6, 12 and 24 h after NMDA injection, mice were killed. At 2, 6 and 12 h, PBS-injected mice or NMDA-injected mice after pretreatment with MK-801(0.01 mg) were also killed. Eyes were dissected immediately, and total RNA was isolated from mouse retina using the AquaPure RNA isolation kit (Bio-Rad Laboratories, Hercules, CA, USA). To remove genomic DNA, the total RNA preparation was treated with deoxyribonuclease I (Invitrogen, Carlsbad, CA, USA). Assay-on-demand primers and probes systems (Applied Biosystems, Foster City, CA, USA) were used to quantify mRNAs for mouse CHOP Assay ID; Mm 00492097 and glyceraldehydes-3-phosphate dehydrogenase (GAPDH Assay ID; Mm 999999 15). These commercially available primers and probes sets, whose sequences were undocumented and whose PCR products were composed to be about 100 base pairs, were widely used (Staller *et al.* 2003; Tokuhiro *et al.* 2003; Roy *et al.* 2004). These primer sets were designed to span exon–exon junctions to eliminate any influence from the presence of contaminant genomic DNA. Real-time RT-PCR was performed with 10 ng of total RNA on an ABI Prism 7000 Sequence Detection System (Applied Biosystems) using the SuperScript One-Step RT-PCR system (Gibco BRL, Grand Island, NY, USA). Total RNA was reverse transcribed into cDNA using one cycle at 50°C for 30 min and one cycle at 95°C for 10 min cDNA was amplified using 40 cycles at 94°C for 15 s and 60°C for 1 min. Fluorescence changes of SYBR Green, the green fluorescent dye were monitored after each cycle. Melting curve analysis was performed (0.5°C/s increase from 55°C to 95°C with continuous fluorescence readings) at the end of 40 cycles to ensure that specific PCR products were obtained. The threshold cycle of fluorescence units was evaluated to quantify the amount of each mRNA level. Each CHOP mRNA level was normalized by the GAPDH mRNA level, and expressed as a mean ± standard deviation. The adjusted CHOP mRNAs after NMDA treatment were statistically analyzed using the ANOVA test. PCR products after 25 cycles for CHOP gene and 25 cycles for GAPDH gene were run by electrophoresis on a 1.5% agarose gel, to check size of PCR (and reaction specificity) and to confirm quantificative results of real-time RT-PCR.

Immunohistochemical staining

NMDA (5 nmol/2 mL) was injected into the vitreous cavity in C57 BL/6 mice. Mice were killed at 2, 6 and 12 h after NMDA injection. As control experiments, mice were treated with either intravitreous PBS injection or intravitreous NMDA injection after 0.01 mg of MK-801 pretreatment. The eyes were immediately enucleated and fixed with 4% paraformaldehyde in PBS. Specimens were dehydrated and embedded into paraffin. Transverse paraffin sections (3-mm thick), including the optic disc, were soaked in xylene, rehydrated in graded ethanols, and then washed with PBS. Sections were treated with 50 mg/mL trypsin and then washed three times. Each section was incubated for 30 min in PBS containing 2% horse serum and 5% skim milk to block non-specific binding. Monoclonal anti-mouse CHOP antibody (Santa Cruz Biotechnology, Santa Cruz, CA, USA) was used at a dilution of 1 : 200 in PBS containing 5% skim milk. Sections were incubated with this antibody overnight at 4°C and then washed three times in PBS. Sections were then incubated with mouse anti-mouse IgG HRP (horseradish peroxidase) antibody (Amersham, Buckinghamshire, UK) for 1 h at room temperature at a dilution of 1 : 500 in PBS. After washing with PBS three times, sections were amplified using the TSA (tyramide signal amplification) biotin system (PerkinElmer, Boston, MA, USA). They were incubated in the biotinyl tyramide

amplification reagent (Perkin Elmer) for 15 min at room temperature and washed with PBS three times. Following this, all slides were incubated with streptavidin Alexa Fluor 488 conjugate (Molecular Probes, Eugene, OR, USA) at a dilution of 1 : 500 in PBS for 30 min in the dark. After washing with PBS, sections were stained with propidium iodide (PI) for 15 min in the dark to illustrate retinal cell distribution and to clear retinal layers such as GCL, INL and outer nuclear layer. After washing with PBS, the number of CHOP-positive cells (in GCL and INL) and the number of PI stained cells (in GCL) were counted at 1.0–1.5 mm from the optic disc using a confocal microscope FV300 (Olympus, Tokyo, Japan), and expressed in millimetres. The percentage of the number of CHOP positive cells for that of PI stained cells was calculated in GCL of mouse retina. One section of each mouse eye was used for counting.

Immunoblot analysis

NMDA (5 nmol/2 mL) was injected into the vitreous cavity in C57 BL/6 mice. At 6 h after NMDA injection, mice were killed. As control experiments, PBS-injected mice or NMDA-injected mice after pretreatment of MK-801 (0.01 mg) were also killed. The retinal tissue was immediately isolated and lysed with lysis buffer containing 1% Nonidet P-40, 150 mM NaCl, 50 mM Tris-HCl (pH 7.4), 1 mM EDTA, 0.25% sodium deoxycholate, and a protease inhibitor tablet, Complete Mini (Roche Molecular Biochemicals, Mannheim, Germany). Lysates were subjected to sodium dodecyl sulfate – polyacrylamide gel electrophoresis (SDS–PAGE) using a 12% Tris-glycine gel (Invitrogen). Following electrophoresis, proteins were transferred to nitrocellulose membranes. Membranes were blocked for 30 min at room temperature using a blocking solution containing 5% skim milk powder and 0.1% Tween-20 in Tris-buffered saline (TBS; pH 7.4), and then incubated with monoclonal anti-mouse CHOP antibody overnight at 4°C diluted 1 : 100 in TBS or monoclonal anti-mouse β-actin antibody (Sigma) diluted 1 : 50000 in TBS for 60 min at room temperature. Membranes were then washed three times and incubated with mouse anti-mouse IgG HRP antibody (Amersham) for 30 min at room temperature at a dilution of 1 : 4000 in TBS. Membranes were washed three times, treated with an enhanced chemiluminescence (ECL) western blotting detection reagent (Amersham) and then exposed to X-ray film. The density of the signal was quantified using NIH (National Institutes of Health) Image 6.2 software and CHOP expression levels were normalized for β-actin. Results are expressed as a mean ± standard deviation for four independent experiments and analyzed statistically using the ANOVA test. An extract of mouse NIH3T3 cells treated with 1 mM thapsigargin (Sigma) for 6 h was used as positive control.

Terminal deoxyribonucleotidyl transferase (TdT)-mediated fluorescein-16-dUTP nick-end labelling (TUNEL) assay

To compare the number of TUNEL-positive cells in wild-type and $CHOP^{-/-}$ mice, a single dose of 2 mL PBS containing 1, 2, 5 or 10 nmol of NMDA was injected into the vitreous cavity. At 24 h after NMDA injection, mice were killed. Eyes were immediately enucleated and fixed with 4% paraformaldehyde in PBS. After specimens were dehydrated and embedded into paraffin, 5-mm thick transverse sections, including the optic disc, were cut. Sections were soaked in xylene to remove paraffin, rehydrated in graded ethanols, and then washed with PBS. The TUNEL assay was performed using the Apoptosis Detection System, Fluorescein (Promega, Madison, WI, USA) according to the manufacturer's protocol. The sections were stained with PI. The number of TUNEL-positive cells (in GCL and INL) and that of PI stained cells (in GCL) were counted at 1.0–1.5 mm from the optic disc under a confocal microscope FV300, and expressed in millimetres. The percentage of the number of TUNEL-positive cells for that of PI stained cells was calculated in the GCL of mouse retina. One section of each mouse eye was used for counting. Data were analyzed using the Student's *t*-test.

Morphometric analysis

Morphometric analysis was conducted as previously described (Inomata *et al.* 2003a,b). $CHOP^{-/-}$ mice and age-matched C57 BL/6 male mice were used in this analysis. Briefly, at 7 days after 2 nmol NMDA injection, mice were killed and eyes were enucleated. The eyes were immersed in 2.5% glutaraldehyde and 2% paraformaldehyde in PBS overnight at 4°C, followed by dehydration and paraffin embedding. Transverse sections 3 mm in thickness, including the optic disc, were prepared from the mouse eyes. Sections were stained with hematoxylin–eosin and photographed at 1.0 mm from the optic disc. The thickness of the inner plexiform layer, INL, outer plexiform layer, and outer nuclear layer was measured and shown as a mean ± standard deviation. The number of residual cells in the GCL (1.0–1.5 mm from the optic disc) was counted and expressed a mean ± standard deviation (in millimetres). One section of each mouse eye was used for counting. Data were analyzed using the Student's *t*-test.

Results

Real-time RT-PCR analysis using total RNA derived from mouse retina was performed to quantify CHOP mRNA expression following NMDA injection (Fig. 1). At 2 h after NMDA treatment, the relative expression level of CHOP mRNA increased to 316 ± 116% of the basal level ($p = 0.005$; 0 vs. 2 h, $p = 0.010$; 2 vs. 24 h, ANOVA). It then decreased to 220 ± 126, 219 ± 116, and 121 ± 68%, at 6, 12 and 24 h after NMDA injection, respectively. After PBS injection, the relative expression level of CHOP mRNA significantly increased to 179 ± 74% of the basal level ($p = 0.010$; 0 vs. 2 h, $p = 0.007$; 2 vs. 6 h, $p = 0.004$; 2 vs. 12 h, ANOVA). After then it was decreased to almost basal level. Similarly, it was significantly increased at 2 h after NMDA treatment in the eyes with pretreatment with MK-801 ($p = 0.007$; 0 vs. 2 h, $p = 0.002$; 2 vs. 6 h, $p = 0.0002$; 2 vs. 12 h, ANOVA). After then, it was decreased to almost basal level. By TUNEL staining assay, TUNEL-positive cells appeared in GCL and INL after 6 h, and then increased up to 24 h after NMDA treatment. However, TUNEL-positive cells were undetectable at any time points (2, 6, 12, 24 h) either in the eyes injected with PBS or in the eyes injected with NMDA after systemic MK-801 pretreatment (data not shown).

In our immunohistochemical analysis, immunoreactivity for CHOP was not conspicuous in the mouse retina under normal conditions (Fig. 2). At 2 h after NMDA injection,

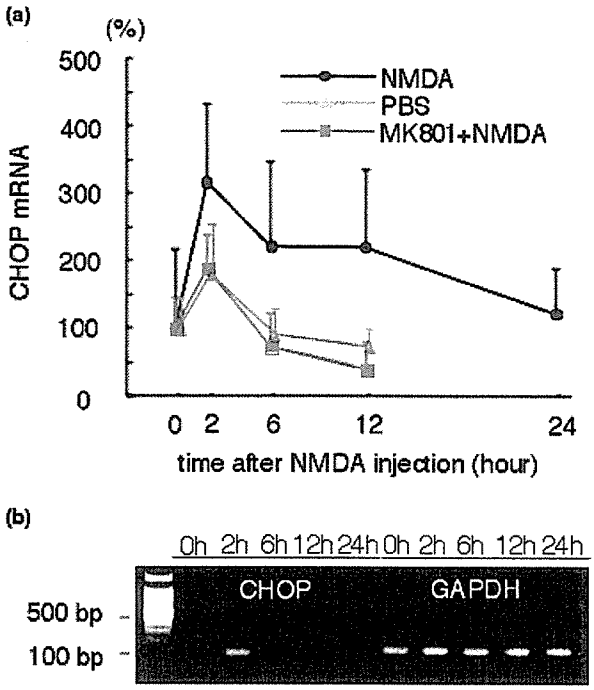

Fig. 1 Expression of CHOP mRNA in mouse retina following NMDA treatment. (a) Real-time RT-PCR analysis of CHOP mRNA was performed after intravitreous NMDA (black) or PBS (green) injection. Some mice were systemically pretreated with MK-801 before intravitreous NMDA injection (red). CHOP mRNA was standardized with GAPDH mRNA. CHOP mRNA was set at 100% in control and expressed as a mean ± standard deviation (n = 5–8). Data were analyzed using the ANOVA test. Asterisks indicate statistically significant differences. (b) RT-PCR experiment of CHOP mRNA and GAPDH mRNA after NMDA injection is shown.

CHOP immunoreactivity was found in cells present in the GCL, and the mean number of CHOP-positive cells in the GCL increased to 6.1 ± 5.6 cells/mm (p = 0.037; 0 vs. 2 h, ANOVA). At 6 h after NMDA treatment, CHOP-positive cells significantly increased to 30.9 ± 1.8 cells/mm in the GCL ($p < 0.0001$; 0 vs. 6 h, 2 vs. 6 h, 6 vs. 12 h, ANOVA). At 12 h after NMDA treatment, the number of CHOP-positive cells decreased to near basal levels (0.6 ± 1.1 cells/mm). In contrast, no CHOP-positive cells were found in control experiments at any time points either with intravitreous injection of PBS or with intravitreous injection of NMDA after systemic MK-801 pretreatment. Additionally, an immunoblot assay was performed to evaluate the relative expression level of CHOP protein (Fig. 3). Under normal conditions, CHOP protein was faintly detected in immunoblot experiments of mouse retinal samples. In both PBS-injected eyes and NMDA-injected eyes after pretreatment with MK-801, the expression level for CHOP protein was almost the same level as that in the untreated eye. After NMDA injection, the relative expression level of CHOP increased to 178 ± 21% of basal levels (p = 0.001; no treatment vs. NMDA, p = 0.0005; PBS vs. NMDA, ANOVA).

The TUNEL assay was performed in the mouse retina of the two strains 24 h after NMDA treatment (Fig. 4). In control experiments using PBS injection, no TUNEL-positive cells were found in C57 BL/6 and CHOP$^{-/-}$ mice. Furthermore, following intravitreous injection of 1 nmol NMDA, only a small number of TUNEL-positive cells were found in the retina of C57 BL/6 and CHOP$^{-/-}$ mice. However, following injection of 2 nmol NMDA, the mean number of TUNEL-positive cells in the GCL of CHOP$^{-/-}$ mice (6.8 ± 3.8 cells/mm) were significantly lower than that of C57 BL/6 mice (18.8 ± 7.4 cells/mm, p = 0.025, Student's t-test). Similarly, the percentage of CHOP positive cells for TUNEL-stained cells in the GCL of CHOP$^{-/-}$ mice (6.4 ± 3.7%) was significantly lower than that of C57 BL/6 mice (16.8 ± 4.9%, p = 0.001, Student's t-test). Furthermore, the number of TUNEL-positive cells in the INL of CHOP$^{-/-}$ mice (5.0 ± 3.7 cells/mm) was significantly lower than the number in C57 BL/6 mice (19.8 ± 4.6 cells/mm, p = 0.001, Student's t-test). After injection of 5 nmol NMDA, the mean number of TUNEL-positive cells in the GCL of CHOP$^{-/-}$ mice (15.3 ± 13.1 cells/mm) was significantly lower than the number in C57 BL/6 mice (36.3 ± 7.5 cells/mm, p = 0.036, Student's t-test). Similarly, the percentage of CHOP-positive cells to TUNEL-stained cells in the GCL of CHOP$^{-/-}$ mice (18.1 ± 14.9%) was significantly lower than that of C57 BL/6 mice (48.9 ± 6.3%, p = 0.001, Student's t-test). However, there was no significant difference in the number of TUNEL-positive cells in the INL of CHOP$^{-/-}$ (37.3 ± 19.3 cells/mm) and C57 BL/6 (44.3 ± 8.2 cells/mm) mice. Additionally, in experiments using a large amount of NMDA (10 nmol), no statistically significant difference was found in either the GCL or INL of these two strains.

Morphological changes were then measured in experiments employing two strains (C57 BL/6 and CHOP$^{-/-}$) following intravitreal injection of 2 nmol NMDA (Fig. 5). In both C57 BL/6 and CHOP$^{-/-}$ mice, the thickness of the inner plexiform layer and INL decreased significantly following NMDA injection. The mean thickness of the IPL in CHOP$^{-/-}$ and in C57 BL/6 mice was 20.3 ± 5.4 and 14.7 ± 4.2 mm, respectively, showing a significant difference (p = 0.018, Student's t-test). Similarly, the mean thickness of the INL in CHOP$^{-/-}$ and in C57 BL/6 mice was 22.7 ± 4.8 and 18.5 ± 3.5 mm, respectively (p = 0.040, Student's t-test). Additionally, in experiments with NMDA treatment, the number of cells in the GCL of CHOP$^{-/-}$ mice was 34.8 ± 11.4 cells/mm, which was higher than that in C57 BL/6 mice (24.1 ± 7.7 cells/mm, p = 0.026, Student's t-test). In contrast, in the outer retinal layers such as the outer plexiform and outer nuclear layers, no difference was observed. Furthermore, in control experiments using intravitreous PBS injection, there was no significant difference in the thickness of any retinal layers of C57 BL/6 and CHOP$^{-/-}$ mice.

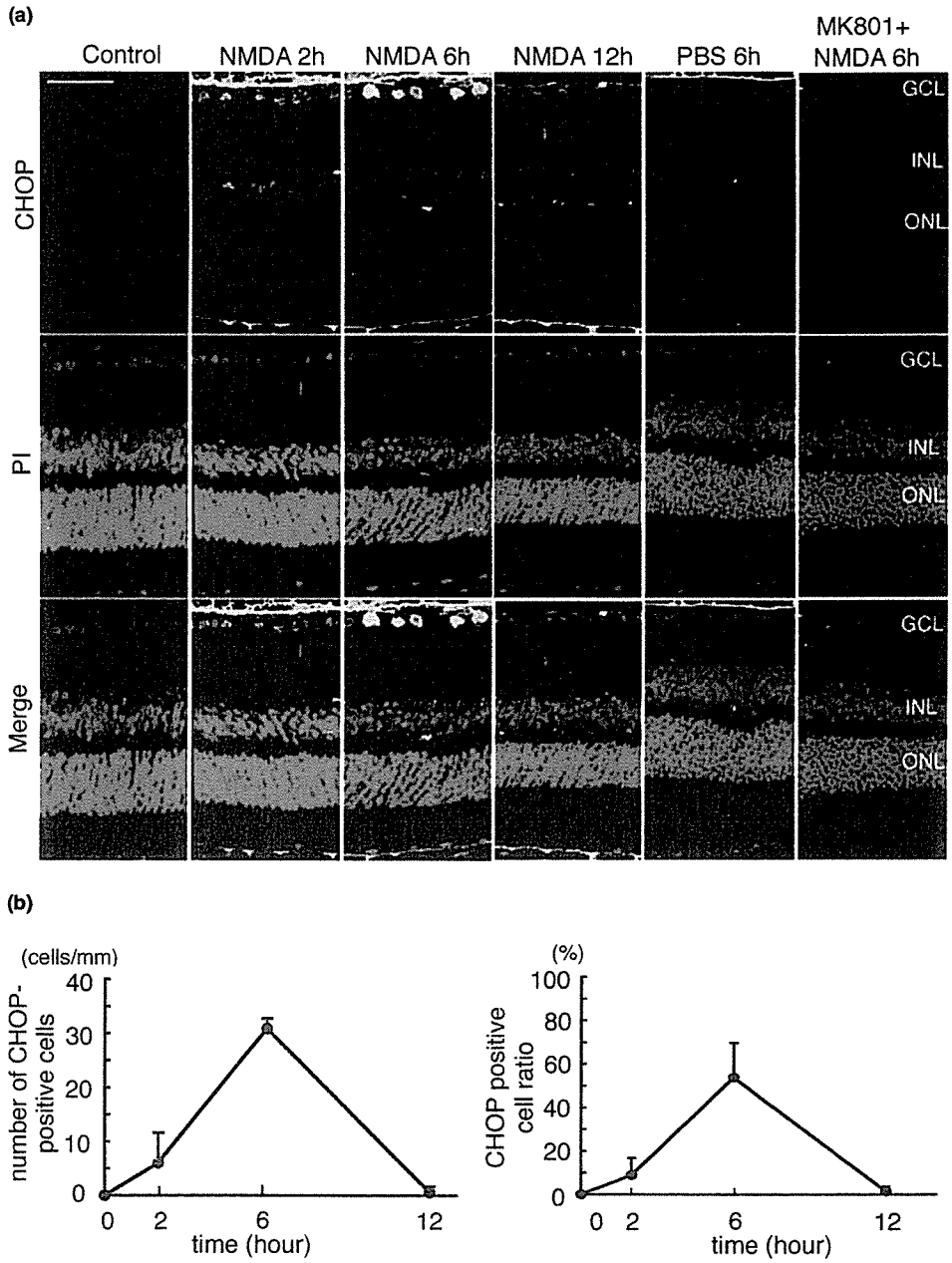

Fig. 2 Immunohistochemical analysis for CHOP protein in mouse retina following NMDA treatment. (a) Immunohistochemical analysis was performed in the eyes with NMDA injection, PBS injection, or NMDA injection after systemic MK-801 treatment. Propidium iodide (PI) staining was also performed. GCL, ganglion cell layer; INL, inner nuclear layer; ONL, outer nuclear layer. Scale bar: 50 mm. (b) The number of CHOP-positive cells was counted and shown as a mean ± standard deviation ($n = 3$). The ratio of CHOP-positive cells/PI stained cells was also shown.

Discussion

In a number of visual-threatening ocular diseases such as ischaemic retinal disease and glaucoma, glutamate toxicity has been regarded as one of the major mechanisms related to retinal neuronal cell death (Kuroiwa *et al.* 1998; Dkhissi *et al.* 1999; Lam *et al.* 1999a,b). This hypothesis is supported by the fact that glutamate receptor antagonists show a neuroprotective effect against some forms of retinal injury and ocular hypertension (glaucoma) in animal experiments (Rosner *et al.* 1997; Chaudhary *et al.* 1998; Sun *et al.* 2001). Recently, notions pertaining to the involvement of ER stress

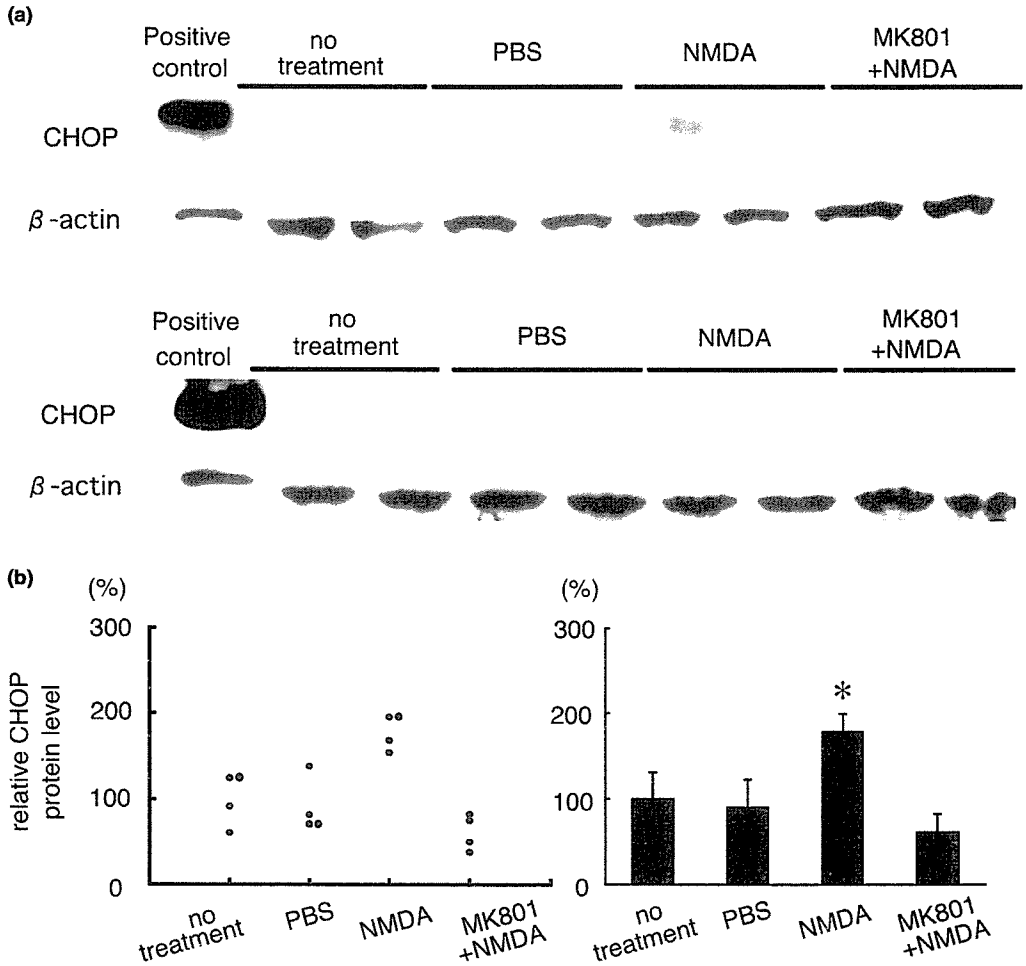

Fig. 3 Immunoblot analysis of CHOP protein following NMDA injection. (a) The homogenates from the retina with no injection, PBS injection, NMDA injection, or NMDA injection after MK-801 pretreatment were subjected to immunoblot analysis. The homogenate from NIH3T3 cells treated with 1 mM thapsigargin was used as a positive control. (b) The amount of CHOP protein was quantified by densitometric analysis and standardized for β-actin. The average of CHOP protein in the retina with no treatment was set at 100%. Data ($n = 4$) were indicated as dot in the left graph. Data are shown as a mean ± standard deviation in the right graph. Data were analyzed using the ANOVA test. Asterisks indicate statistically significant differences.

in neuronal damage have received much attention by investigators. The molecular mechanisms involved have been shown to play an important role in neurodegenerative disorders such as Alzheimer's disease (Mattson and Chan 2003; Katayama *et al.* 2004; Pereira *et al.* 2004), Parkinson's disease (Imai *et al.* 2000; Chen *et al.* 2004), polyglutamine diseases (Kouroku *et al.* 2002; Nishitoh *et al.* 2002; Takeda *et al.* 2002), and brain ischaemia (DeGracia and Montie 2004; Kitano *et al.* 2004). To date, however, there has been no investigation concerning the involvement of ER stress in the pathogenesis of retinal injury (or glaucoma). Among the ER stress-related molecules, CHOP is known to be highly induced in response to ER stress and is implicated to play a role in apoptosis (Ron *et al.* 1992). Induction of this molecule is thought to play an important role in the pathway of ER stress-mediated apoptosis (Kawahara *et al.* 2001; Oyadomari *et al.* 2001; Gotoh *et al.* 2002; Oyadomari *et al.* 2002a,b; Gotoh *et al.* 2004; Oyadomari *et al.* 2004; Tajiri *et al.* 2004; Tsutsumi *et al.* 2004). A previous report of gene-array analysis on NMDA-induced retinal injury showed an up-regulation of some molecules, including a 3.7-fold increase in CHOP (Laabich *et al.* 2001). This exhaustive assay, using microarray, already predicted the importance of the CHOP gene in NMDA retinal injury. In the present study, we clearly showed the important role of the CHOP gene in neuronal cell death in NMDA-induced retinal damage.

Our results from a series of experiments showed that CHOP is up-regulated in eyes with NMDA-induced retinal injury. Real-time RT-PCR experiments showed that the relative level of CHOP mRNA expression peaked at 2 h after

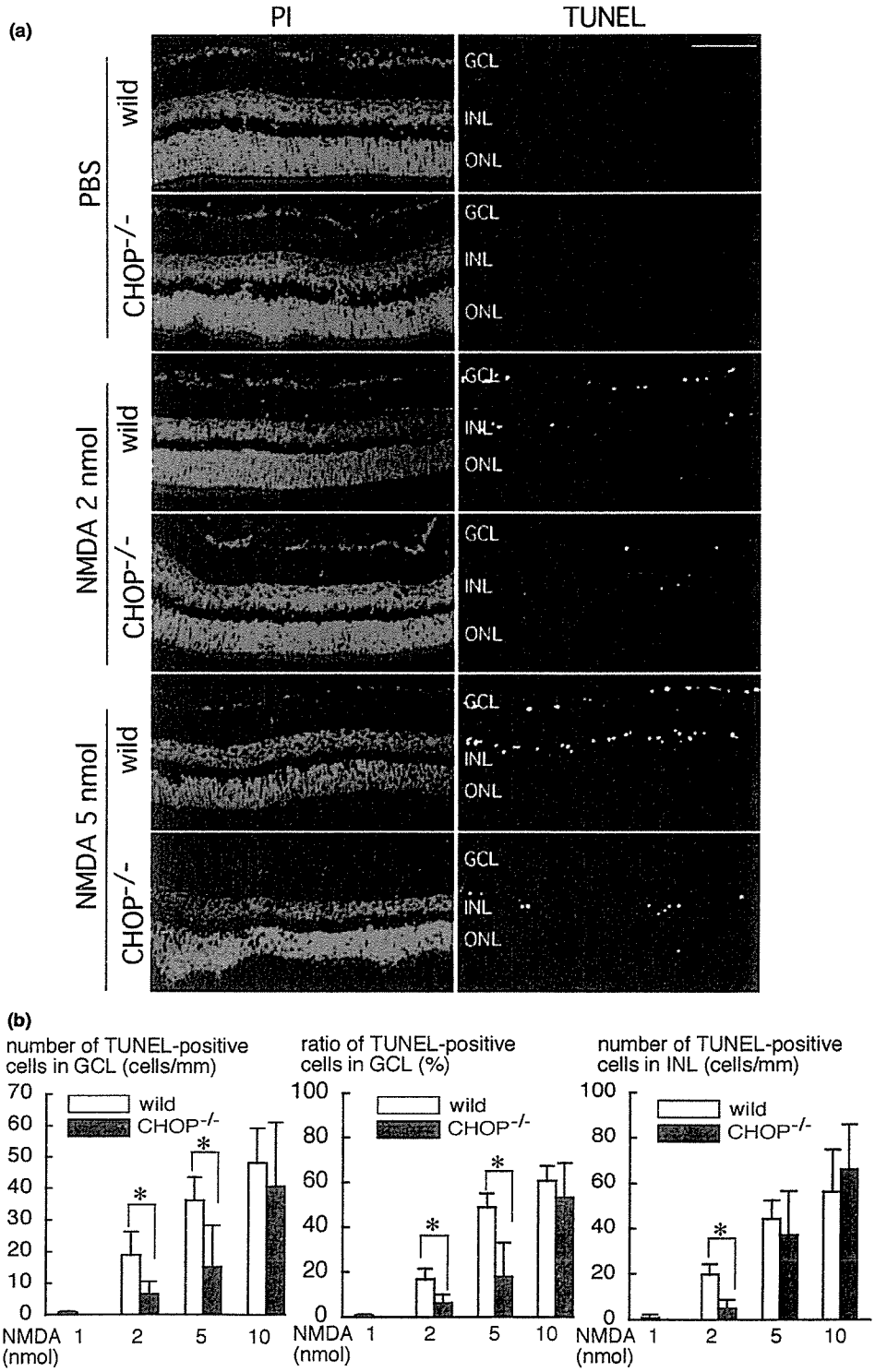

Fig. 4 (a) Terminal deoxyribonucleotidyl transferase (TdT)- mediated fluorescein-16-dUTP nick-end labelling (TUNEL) staining of wild-type and CHOP$^{-/-}$ mouse retina at 24 h after NMDA treatment. Propidium iodide (PI) staining was also performed. Scale bar: 50 mm. GCL, ganglion cell layer; INL, inner nuclear layer; ONL, outer nuclear layer. (b) The number of TUNEL-positive cells in GCL and that in INL were counted and expressed as a mean ± standard deviation ($n = 4$–6). The ratio of TUNEL-positive cells/PI stained cells was calculated and shown. Data were analyzed using the Student's *t*-test.

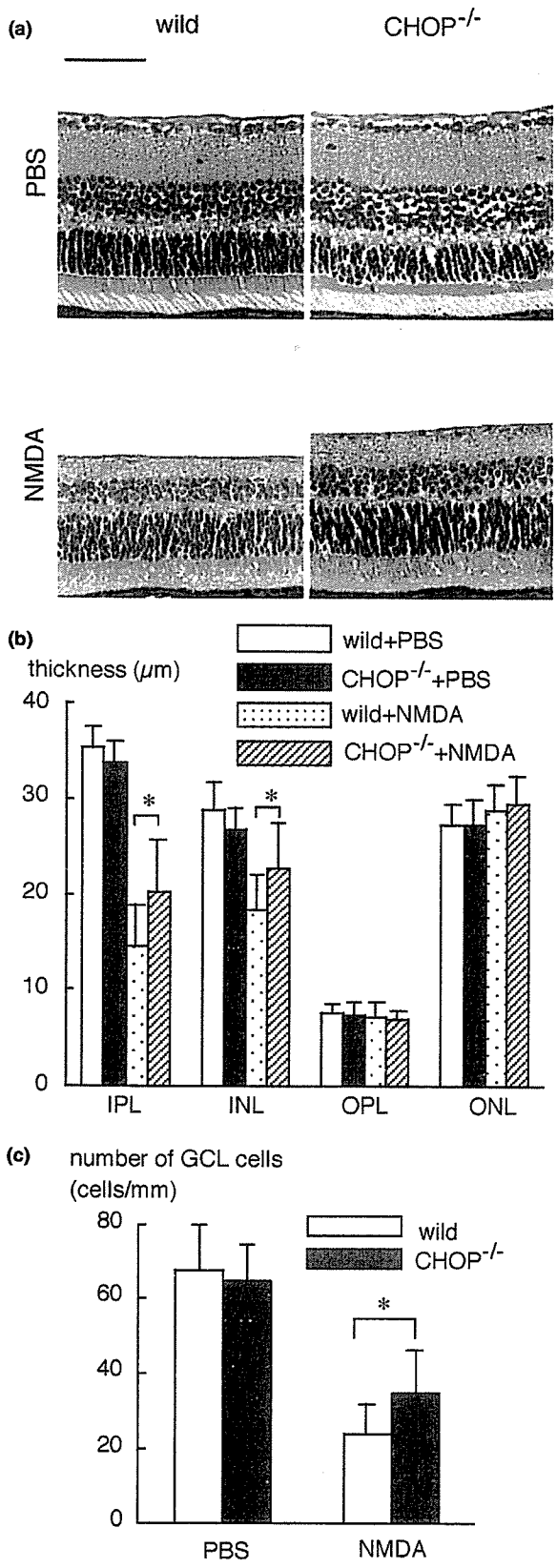

Fig. 5 Morphological analysis of wild-type and CHOP$^{-/-}$ mouse retina at 7 days after 2 nmol NMDA treatment. (a) Paraffin sections stained with hematoxylin-eosin. GCL, ganglion cell layer; IPL, inner plexiform layer; INL, inner nuclear layer; OPL, outer plexiform layer; ONL, outer nuclear layer; PR, photoreceptor. (b) The thickness of retinal layers such as IPL, INL, OPL and ONL was measured and shown as a mean ± standard deviation ($n = 10$). Data were analyzed using the Student's *t*-test. Scale bar: 50 mm. (c) The number of residual cells in the ganglion cell layer was counted and shown as a mean ± standard deviation. Data were analyzed using the Student's *t*-test.

NMDA injection. Given that CHOP immunoreactivity in retinal sections of the GCL peaked at 6 h after NMDA treatment, up-regulated expression of the CHOP protein can be expected to follow the increased expression of CHOP mRNA. However, in either of the eyes with PBS injection or those with NMDA injection after MK-801 treatment, mRNA for CHOP was induced in our real-time RT-PCR study, but CHOP protein induction was not observed in our immunohistochemical and immunoblot studies. It seemed that inductions of CHOP protein in these control eyes were under the detection limits of our assays. All these results may imply a contribution of CHOP to the onset and progression of apoptotic cell death in retinal tissue caused by NMDA, as TUNEL-positive cells appeared after 6 h, and then increased during the following 24 h after NMDA treatment.

It was somewhat surprising that CHOP protein was induced strongly in retinal cells of the GCL but little expressed in retinal cells of INL, although TUNEL-positive cells were observed in both the GCL and INL. A number of retinal ganglion cells are located in the GCL, and apoptosis of these cells plays a key role in the pathogenesis of glaucoma, a major cause of blindness (Quigley *et al.* 1995; Rosenbaum *et al.* 1998). It was known that susceptibility for ER stress differs markedly from cell to cell, and organ to organ. The pancreatic β-cell, having abundant ER in the cytoplasm and synthesizing insulin vigorously, is one of the most susceptible cells for ER stress (Oyadomari *et al.* 2001). Ultrastructural observations have demonstrated that the cytoplasm of retinal ganglion cells contains abundant ER, suggesting active synthesis of 'secretary' proteins (Sigelman *et al.* 1982). Retinal ganglion cells might be more susceptible to ER stress than other retinal cells in INL. Our observation of increased expression of CHOP protein in retinal cells of GCL may be associated with these cell characteristics of retinal ganglion cells.

ER functions as an intracellular calcium store and plays an important role in Ca^{2+} homeostasis by pumping Ca^{2+} via the ER rumen (Paschen 2003). NMDA caused Ca^{2+} influx from the ER to cytosol, and resulted in ER Ca^{2+} depletion and ER stress (Paschen *et al.* 2001). ER stress followed by Ca^{2+} depletion induces the CHOP gene (Oyadomari *et al.* 2004). In our report, overexpression of calreticulin, a major binding protein in ER, increases ER Ca^{2+} stores and protects against

nitric oxide-induced (CHOP-mediated) apoptosis (Oyadomari *et al.* 2001). As mentioned above, it was thought that NMDA depletes ER Ca^{2+} stores, leads ER dysfunction and CHOP protein induction in retinal cells in the GCL. However, the precise apoptosis cascade downstream of CHOP is not well known. It was reported that overexpression of Bcl-2 blocked CHOP-induced apoptosis (Matsumoto *et al.* 1996) and overexpression of CHOP leads to a decrease in Bcl-2 protein (McCullough *et al.* 2001). We recently found that CHOP-induced apoptosis in RAW 264.7 macrophages is mediated by translocation of Bax from the cytosol to the mitochondria (Gotoh *et al.* 2004). Further study is required to reveal in detail the cascade of CHOP downstream.

Morphological abnormality was not seen in adult ocular tissues of $CHOP^{-/-}$ mice. $CHOP^{-/-}$ mice were reported to display normal development and fertility (Zinszner *et al.* 1998; Oyadomari *et al.* 2001). Similarly, normal development and fertility was reported in other ER stress-related gene knockout mice, such as caspase $12^{-/-}$ mice and ASK1 (apoptosis signal-regulating kinase)$^{-/-}$ mice (Nakagawa *et al.* 2000; Tobiume *et al.* 2001). Therefore, knockout of the CHOP gene would probably not cause serious developmental abnormalities, because this gene might not have such an important role in ocular development. However, our present study demonstrated that $CHOP^{-/-}$ mice are more resistant to retinal injury when the injury was caused with low doses (2–5 nmol) of NMDA. Our results showed that the neuroprotective effects in CHOP-deficient mice against NMDA-induced retinal injury were limited. We speculate that other CHOP-independent apoptosis cascades, such as oxidative stress and DNA damage, might cause neuronal cell death in $CHOP^{-/-}$ mice. In the experiments using pancreatic b-cells, low doses of nitric oxide depleted ER Ca^{2+}, led to ER dysfunction, induced CHOP protein, and resulted in apoptosis. As the dose of nitric oxide was increased, other apoptosis molecules, such as DNA damage-related protein p53, were induced in addition to CHOP protein (Oyadomari *et al.* 2001). In addition, in $CHOP^{-/-}$ mice, pancreatic b-cells were more resistant to nitric oxide-induced apoptosis than those from wild-type mice (Oyadomari *et al.* 2001). Targeted disruption of the CHOP gene could delay b-cell apoptosis and diabetes mellitus in insulin 2 mutation diabetes mice (Oyadomari *et al.* 2002a). Furthermore, $CHOP^{-/-}$ mice were more resistant to neuronal cell death in brain ischaemia (Tajiri *et al.* 2004). However, unlike $CHOP^{-/-}$ mice, pancreatic islets derived from $CHOP^{+/-}$ mice were not resistant to nitric oxide-induced apoptosis (Oyadomari *et al.* 2001), and $CHOP^{+/-}$ mice could not block or delay the development of diabetes caused by insulin mutation (Oyadomari *et al.* 2002a).

In conclusion, our results indicated that intravitreous NMDA injection induced CHOP expression and led to apoptosis in the GCL. Disruption of the CHOP gene gave resistance to NMDA-induced retinal damage. We propose that the ER stress–CHOP pathway is a potential target that may prevent retinal neuronal cell apoptosis induced by excitatory amino acids.

Acknowledgements

We thank Shizuo Akira (Osaka University) for providing the $CHOP^{-/-}$ mice. This work was supported in part by a Grant-in-Aid for Scientific Research from the Ministry of Education, Science, Sports and Culture, Japan and from the Ministry of Health and Welfare, Japan. Commercial relationship policy: N.

References

Alberts B., Johnson A., Lewis J., Raff M., Roberts K. and Walter P. (2002) The endoplasmic reticulum, in *Molecular Biology of the Cell*, 4th edn. pp. 689–709. Garland Science, New York.

Barone M. V., Crozat A., Tabaee A., Philipson L. and Ron D. (1994) CHOP(GADD153) and its oncogenic variant, TLS-CHOP, have opposing effects on the induction of G1/S arrest. *Genes Dev.* **8**, 453–464.

Chaudhary P., Ahmed F. and Sharma S. C. (1998) MK801-a neuroprotectant in rat hypertensive eyes. *Brain Res.* **792**, 154–158.

Chen G., Bower K. A., Ma C., Fang S., Thiele C. J. and Luo J. (2004) Glycogen synthase kinase 3 (GSK3b) mediates 6-hydroxydopamine-induced neuronal death. *FASEB J.* **18**, 1162–1164.

DeGracia D. J. and Montie H. L. (2004) Cerebral ischemia and the unfolded protein response. *J. Neurochem.* **91**, 1–8.

Dkhissi O., Chanut E., Wasowicz M., Savoldelli M., Nguyen-Legros J., Minvielle F. and Versaux-Botteri C. (1999) Retinal TUNEL-positive cells and high glutamate levels in vitreous humor of mutant quail with a glaucoma-like disorder. *Invest. Ophthalmol. Vis. Sci.* **40**, 990–995.

Farrar G. J., Kenna P. F. and Humphries P. (2002) On the genetics of retinitis pigmentosa and on mutation-independent approaches to therapeutic intervention. *EMBO J.* **21**, 857–864.

Gotoh T., Oyadomari S., Mori K. and Mori M. (2002) Nitric oxide-induced apoptosis in RAW 264.7 macrophages is mediated by endoplasmic reticulum stress pathway involving ATF6 and CHOP. *J. Biol. Chem.* **277**, 12 343–12 350.

Gotoh T., Terada K., Oyadomari S. and Mori M. (2004) Hsp70-DnaJ chaperone pair prevents nitric oxide- and CHOP-induced apoptosis by inhibiting translocation of Bax to mitochondria. *Cell Death Differ.* **11**, 390–402.

Hajnoczky G., Davies E. and Madesh M. (2003) Calcium signaling and apoptosis. *Biochem. Biophys. Res. Commun.* **304**, 445–454.

Imai Y., Soda M. and Takahashi R. (2000) Parkin suppresses unfolded protein stress-induced cell death through its E3 ubiquitin-protein ligase activity. *J. Biol. Chem.* **275**, 35 661–35 664.

Inomata Y., Hirata A., Yonemura N., Koga T., Kido N. and Tanihara H. (2003a) Neuroprotective effects of interleukin-6 on NMDA-induced rat retinal damage. *Biochem. Biophys. Res. Commun.* **302**, 226–232.

Inomata Y., Hirata A., Koga T., Kimura A., Singh D. P., Shinohara T. and Tanihara H. (2003b) Lens epithelium-derived growth factor: neuroprotection on rat retinal damage induced by *N*-methyl-D-aspartate. *Brain Res.* **991**, 163–170.

Joo C. K., Choi J. S., Ko H. W., Park K. Y., Sohn S., Chun M. H., Oh Y. J. and Gwag B. J. (1999) Necrosis and apoptosis after retinal ischemia: involvement of NMDA-mediated excitotoxicity and p53. *Invest. Ophthalmol. Vis. Sci.* **40**, 713–720.

Katayama T., Imaizumi K., Manabe T., Hitomi J., Kudo T. and Tohyama M. (2004) Induction of neuronal death by ER stress in Alzheimer's disease. *J. Chem. Neuroanat.* **28**, 67–78.

Kaufman R. J., Scheuner D., Schroder M., Shen X., Lee K., Liu C. Y. and Arnold S. M. (2002) The unfolded protein response in nutrient sensing and differentiation. *Nat. Rev. Mol. Cell Biol.* **3**, 411–421.

Kawahara K., Oyadomari S., Gotoh T., Kohsaka S., Nakayama H. and Mori M. (2001) Induction of CHOP and apoptosis by nitric oxide in p53-deficient microglial cells. *FEBS Lett.* **506**, 135–139.

Kerrigan L. A., Zack D. J., Quigley H. A., Smith S. D. and Pease M. E. (1997) TUNEL-positive ganglion cells in human primary open-angle glaucoma. *Arch. Ophthalmol.* **115**, 1031–1035.

Kitano H., Nishimura H., Tachibana H., Yoshikawa H. and Matsuyama T. (2004) ORP150 ameliorates ischemia/reperfusion injury from middle cerebral artery occlusion in mouse brain. *Brain Res.* **1015**, 122–128.

Kouroku Y., Fujita E., Jimbo A. *et al.* (2002) Polyglutamine aggregates stimulate ER stress signals and caspase-12 activation. *Hum. Mol. Genet.* **11**, 1505–1515.

Kuroiwa S., Katai N., Shibuki H., Kurokawa T., Umihira J., Nikaido T., Kametani K. and Yoshimura N. (1998) Expression of cell cycle-related genes in dying cells in retinal ischemic injury. *Invest. Ophthalmol. Vis. Sci.* **39**, 610–617.

Laabich A., Li G. and Cooper N. G. (2001) Characterization of apoptosis-genes associated with. NMDA mediated cell death in the adult rat retina. *Brain Res. Mol. Brain Res.* **91**, 34–42.

Lam T. T., Abler A. S., Kwong J. M. and Tso M. O. (1999a) *N*-methyl-D-aspartate (NMDA)-induced apoptosis in rat retina. *Invest. Ophthalmol. Vis. Sci.* **40**, 2391–2397.

Lam T. T., Abler A. S. and Tso M. O. (1999b) Apoptosis and caspases after ischemia-reperfusion injury in rat retina. *Invest. Ophthalmol. Vis. Sci.* **40**, 967–975.

Matsumoto M., Minami M., Takeda K., Sakao Y. and Akira S. (1996) Ectopic expression of CHOP (GADD153) induces apoptosis in M1 myeloblastic leukemia cells. *FEBS Lett.* **395**, 143–147.

Mattson M. P. and Chan S. L. (2003) Neuronal and glial calcium signaling in Alzheimer's disease. *Cell Calcium* **34**, 385–397.

McCullough K. D., Martindale J. L., Klotz L. O., Aw T. Y. and Holbrook N. J. (2001) Gadd 153 sensitizes cells to endoplasmic reticulum stress by down-regulating Bcl2 and perturbing the cellular redox state. *Mol. Cell Biol.* **21**, 1249–1259.

Nakagawa T., Zhu H., Morishima N., Li E., Xu J., Yankner B. A. and Yuan J. (2000) Caspase-12 mediates endoplasmic-reticulum-specific apoptosis and cytotoxicity by amyloid-β. *Nature* **403**, 98–103.

Nishitoh H., Matsuzawa A., Tobiume K., Saegusa K., Takeda K., Inoue K., Hori S., Kakizuka A. and Ichijo H. (2002) ASK1 is essential for endoplasmic reticulum stress-induced neuronal cell death triggered by expanded polyglutamine repeats. *Genes Dev.* **16**, 1345–1355.

Oyadomari S. and Mori M. (2004) Roles of CHOP/GADD153 in endoplasmic reticulum stress. *Cell Death Differ.* **11**, 381–389.

Oyadomari S., Takeda K., Takiguchi M., Gotoh T., Matsumoto M., Wada I., Akira S., Araki E. and and. Mori M. (2001) Nitric oxide-induced apoptosis in pancreatic β cells is mediated by the endoplasmic reticulum stress pathway. *Proc. Natl Acad. Sci. USA* **98**, 10 845–10 850.

Oyadomari S., Koizumi A., Takeda K., Gotoh T., Akira S., Araki E. and Mori M. (2002a) Targeted disruption of the Chop gene delays endoplasmic reticulum stress-mediated diabetes. *J. Clin. Invest.* **109**, 525–532.

Oyadomari S., Araki E. and Mori M. (2002b) Endoplasmic reticulum stress-mediated apoptosis in pancreatic b-cells. *Apoptosis* **7**, 335–345.

Paschen W. (2003) Endoplasmic reticulum: a primary target in various acute disorders and degenerative diseases of the brain. *Cell Calcium* **34**, 365–383.

Paschen W. and Frandsen A. (2001) Endoplasmic reticulum dysfunction – a common denominator for cell injury in acute and degenerative diseases of the brain? *J. Neurochem.* **79**, 719–725.

Pereira C., Ferreiro E., Cardoso S. M. and de Oliveira C. R. (2004) Cell degeneration induced by amyloid-b peptides: implications for Alzheimer's disease. *J. Mol. Neurosci.* **23**, 97–104.

Quigley H. A., Nickells R. W., Kerrigan L. A., Pease M. E., Thibault D. J. and Zack D. J. (1995) Retinal ganglion cell death in experimental glaucoma and after axotomy occurs by apoptosis. *Invest. Ophthalmol. Vis. Sci.* **36**, 774–786.

Reme C. E., Grimm C., Hafezi F., Marti A. and Wenzel A. (1998) Apoptotic cell death in retinal degenerations. *Prog. Retin. Eye Res.* **17**, 443–464.

Ron D. and Habener J. F. (1992) CHOP, a novel developmentally regulated nuclear protein that dimerizes with transcription factors C/EBP and LAP and functions as a dominant-negative inhibitor of gene transcription. *Genes Dev.* **6**, 439–453.

Rosenbaum D. M., Rosenbaum P. S., Gupta H., Singh M., Aggarwal A., Hall D. H., Roth S. and Kessler J. A. (1998) The role of the p53 protein in the selective vulnerability of the inner retina to transient ischemia. *Invest. Ophthalmol. Vis. Sci.* **39**, 2132–2139.

Rosner M., Solberg Y., Turetz J. and Belkin M. (1997) Neuroprotective therapy for argon-laser induced retinal injury. *Exp. Eye Res.* **65**, 485–495.

Roy N. S., Nakano T., Keyoung H. M. *et al.* (2004) Telomerase immortalization of neuronally restricted progenitor cells derived from the human fetal spinal cord. *Nat. Biotechnol.* **22**, 297–305.

Sigelman J. and Ozanics V. (1982) Retina, in *Ocular Anatomy, Embryology, and Teratology* (Jakobiec, F. A., ed.), pp. 478–481. Harper and Row, Philadelphia.

Staller P., Sulitkova J., Lisztwan J., Moch H., Oakeley E. J. and Krek W. (2003) Chemokine receptor CXCR4 downregulated by von Hippel-Lindau tumour suppressor pVHL. *Nature* **425**, 307–311.

Sun Q., Ooi V. E. and Chan S. O. (2001) *N*-methyl-D-aspartate-induced excitotoxicity in adult rat retina is antagonized by single systemic injection of MK-801. *Exp. Brain Res.* **138**, 37–45.

Tajiri S., Oyadomari S., Yano S., Morioka M., Gotoh T., Hamada J. I., Ushio Y. and Mori M. (2004) Ischemia-induced neuronal cell death is mediated by the endoplasmic reticulum stress pathway involving CHOP. *Cell Death Differ.* **11**, 403–415.

Takeda K., Matsuzawa A., Nishitoh H., Tobiume K., Kishida S., Ninomiya-Tsuji J., Matsumoto K. and Ichijo H. (2002) ASK1 is essential for endoplasmic reticulum stress-induced neuronal cell death triggered by expanded polyglutamine repeats. *Genes Dev.* **16**, 1345–1355.

Tobiume K., Matsuzawa A., Takahashi T. *et al.* (2001) ASK1 is required for sustained activations of JNK/p38 MAP kinases and apoptosis. *EMBO Report* **2**, 222–228.

Tokuhiro S., Yamada R., Chang X. *et al.* (2003) An intronic SNP in a RUNX1 binding site of. SLC22A4, encoding an organic cation transporter, is associated with rheumatoid arthritis. *Nat. Genet.* **35**, 341–348.

Tsutsumi S., Gotoh T., Tomisato W. *et al.* (2004) Endoplasmic reticulum stress response is involved in nonsteroidal anti-inflammatory drug-induced apoptosis. *Cell Death Differ.* **11**, 1009–1016.

Wax M. B., Tezel G. and Edward P. D. (1998) Clinical and ocular histopathological findings in a patient with normal-pressure glaucoma. *Arch. Ophthalmol.* **116**, 993–1001.

Zinszner H., Kuroda M., Wang X., Batchvarova N., Lightfoot R. T., Remotti H., Stevens J. L. and Ron D. (1998) CHOP is implicated in programmed cell death in response to impaired function of the endoplasmic reticulum. *Genes Dev.* **12**, 982–995.

STEM CELLS®
Tissue-Specific Stem Cells

Activation of Canonical Wnt Pathway Promotes Proliferation of Retinal Stem Cells Derived from Adult Mouse Ciliary Margin

TOSHIHIRO INOUE,[a,b] TETSUSHI KAGAWA,[b,c] MIKIKO FUKUSHIMA,[a] TAKESHI SHIMIZU,[b] YUTAKA YOSHINAGA,[b] SHINJI TAKADA,[d] HIDENOBU TANIHARA,[a] TETSUYA TAGA[b]

[a]Department of Ophthalmology and Visual Science, Graduate School of Medical Sciences and [b]Department of Cell Fate Modulation, Institute of Molecular Embryology and Genetics, Kumamoto University Graduate School of Medical Science, Kumamoto, Japan; [c]Division of Active Transport, National Institute for Physiological Sciences, Okazaki, Japan; [d]Center for Integrative Bioscience, Okazaki National Research Institutes, Okazaki, Japan

Key Words. Retina • Stem cell • Wnt • Proliferation • Ciliary margin • Beta-Catenin • GSK3 inhibitor • Fibroblast growth factor

ABSTRACT

Adult retinal stem cells represent a possible cell source for the treatment of retinal degeneration. However, only a small number of stem cells reside in the ciliary margin. The present study aimed to promote the proliferation of adult retinal stem cells via the Wnt signaling pathway. Ciliary margin cells from 8-week-old mice were dissociated and cultured to allow sphere colony formation. Wnt3a, a glycogen synthase kinase (GSK) 3 inhibitor, fibroblast growth factor (FGF) 2, and a FGF receptor inhibitor were then applied in the culture media. The primary spheres were dissociated to prepare either monolayer or secondary sphere cultures. Wnt3a increased the size of the primary spheres and the number of Ki-67–positive proliferating cells in monolayer culture. The Wnt3a-treated primary sphere cells were capable of self-renewal and gave rise to fourfold the number of secondary spheres compared with nontreated sphere cells. These cells also retained their multilineage potential to express several retinal markers under differentiating culture conditions. The Wnt3a-treated cells showed nuclear accumulation of β-catenin, and a GSK3 inhibitor, SB216763, mimicked the mitogenic activity of Wnt3a. The proliferative effect of SB216763 was attenuated by an FGF receptor inhibitor but was enhanced by FGF2, with Ki-67–positive cells reaching over 70% of the total cells. Wnt3a and SB216763 promoted the proliferation of retinal stem cells, and this was partly dependent on FGF2 signaling. A combination of Wnt and FGF signaling may provide a therapeutic strategy for in vitro expansion or in vivo activation of adult retinal stem cells. STEM CELLS *2006;24:95–104*

INTRODUCTION

The ciliary marginal zone is widely known to contain immature retinal cells that continue to divide throughout life in both amphibians and fish [1–7]. Recently, a limited number of ciliary margin cells in adult rodents were demonstrated to sustain stem cell characteristics in vitro [8, 9]. From a therapeutic viewpoint, stem cells residing in an adult tissue, if able to be expanded in vitro or activated in vivo, have a significant advantage in autologous transplantation or activation of endogenous stem cells because they can overcome immune rejection and the ethical

Correspondence: Tetsuya Taga, Ph.D., Department of Cell Fate Modulation, Institute of Molecular Embryology and Genetics, Kumamoto University, 2-2-1 Honjo, Kumamoto-city, Japan. Telephone: 81-96-3736614; Fax: 81-96-3736614; e-mail: taga@kaiju.medic.kumamoto-u.ac.jp. Received March 18, 2005; accepted for publication June 28, 2005.
1066-5099/2006/$12.00/0 doi: 10.1634/stemcells.2005-0124

concerns associated with using embryonic or neonatal tissues. Therefore, retinal stem cells in the adult ciliary margin have been highlighted as a possible cell source for stem cell therapies. However, it is debatable whether these cells can provide the copious stem cell pools required for therapy because a single primary sphere colony can only generate six to eight secondary spheres in the presence of fibroblast growth factor (FGF) 2 [9]. In addition, a limited number of primary spheres can be generated from individual adult eyes; only approximately 55 spheres were obtained from individual adult rodent eyes [9], and these spheres showed lower and restricted proliferation potential compared with neural stem cells derived from the adult subventricular zone [10]. Hence, improved and efficient strategies to expand retinal stem cells are required.

Wnt proteins are secreted lipid-modified signaling molecules that regulate cell proliferation and cell fate in various tissues in vertebrate embryos and can activate different intracellular signaling cascades, including the canonical pathway, c-Jun N-terminal kinase pathway, Ca^{2+} pathway, and focal adhesion kinase pathway (reviewed by Pandur et al. [11]). In the canonical pathway, Wnt protein binding to Frizzled (Fzd) and low-density lipoprotein receptor–related proteins (LRP) causes inactivation of glycogen synthase kinase (GSK) 3β and Axin, respectively. The inactivation of these proteins stabilizes β-catenin, which subsequently accumulates in the cell nucleus and activates the transduction of target genes that are crucial in the G1–S-phase transition, such as cyclin D1 or c-Myc (reviewed by Willert et al. [12]). Therefore, the canonical Wnt pathway contributes to cell proliferation in different types of stem cells [13–17].

During eye development in the chick, various components of Wnt signaling are expressed. Kubo et al. [18] demonstrated that Wnt2b can promote the proliferation of chick embryonic ciliary margin cells that can yield differentiated retinal progeny through activation of the canonical pathway. This finding encouraged us to explore whether Wnt signaling could promote the proliferation of adult retinal stem cells from the mammalian ciliary margin. In the present study, we demonstrate that Wnt3a increased the size of the spheres derived from ciliary margin. Wnt3a also increased the number of cells expressing Ki-67 and bromodeoxyuridine (BrdU) incorporation in triturated sphere cell cultures. More importantly, Wnt3a-treated sphere cells retained multipotency and formed a greater number of secondary spheres than nontreated cells, indicating that Wnt signaling functions on self-renewal of retinal stem cells (secondary sphere-forming ability). We further suggest that the Wnt3a-mediated increase in self-renewal involved the canonical pathway. Interestingly, the mitogenic effect of Wnt signaling was enhanced by exogenous FGF2 and attenuated by a FGF receptor inhibitor. Our results provide a basis for the development of useful strategies for the in vitro expansion of adult retinal stem cells.

Materials and Methods

Isolation and Culture

Eight-week-old C57Bl6 mice and green fluorescent protein (GFP) transgenic mice were used to prepare adult retinal stem cells as previously reported [9]. All studies were conducted in accordance with the guidelines of the Kumamoto University Center for Animal Resources and Development. Dissociated cells were cultured at clonal density for 5 days on six-well dishes (Nunc, Naperville, IL, http://www.nuncbrand.com) precoated with poly-HEME (Sigma-Aldrich, St. Louis, http://www.sigmaaldrich.com) in Dulbecco's modified Eagle's medium/F-12 medium (Invitrogen, Carlsbad, CA, http://www.invitrogen.com) containing B27 (Invitrogen) and various supplements: FGF2 (recombinant human FGF2; R&D Systems, Minneapolis, http://www.rndsystems.com), Wnt3a (recombinant mouse Wnt3a; catalog no. 1324-WN; R&D Systems), or SB216763 (Biomol Research Laboratories, Plymouth Meeting, PA, http://www.biomol.com). The cells were then triturated with enzymatic solution [9], replated on chamber slides (Nunc) precoated with poly-L-ornithine (Sigma-Aldrich) and fibronectin (Life Technologies, Gaithersburg, MD), and cultured for 2 days in B27/DMEM/F-12 containing various supplements: FGF2, Wnt3a, SB216763, Fzd-8-CRD (recombinant mouse Fzd-8/Fc chimera; R&D Systems), or SU5402 (EMD biosciences, San Diego, http://splash.emdbiosciences.com). The S-phase cells in these culture condition were further monitored by BrdU incorporation. After 2-day cultures with or without Wnt3a, the cells were pulse labeled with 10 μM BrdU for 4 hours, incubated in BrdU-free media for an additional 2 hours, and fixed for the immunochemical analyses. For secondary sphere formation, B27/DMEM/F-12 containing FGF2 and epidermal growth factor (EGF) (recombinant human EGF; R&D Systems) was used. To promote retinal cell differentiation, triturated cells were cultured for 7 days as previously described [9]. All cultures were maintained at 37°C in 5% CO_2.

Reverse Transcription–Polymerase Chain Reaction

Total RNA was isolated from sphere cells using Trizol (Invitrogen). Reverse transcription was performed on 2 μg of RNA using Superscript II (Invitrogen) according to the manufacturer's protocol. Reverse transcription products were amplified by polymerase chain reaction (PCR) using KOD-plus (Toyobo, Osaka, Japan, http://www.toyobo.co.jp) and gene-specific primers [19–22] under standard reaction conditions with an initial 2-minute denaturation step followed by 24 to 30 cycles of 94°C for 15 seconds, 58°C for 30 seconds, and 68°C for 60 seconds.